

Global Biogeochemical Cycles

RESEARCH ARTICLE

10.1029/2017GB005798

Key Points:

- Reclaimed mountaintop removal coal mines have among the highest weathering rates in the world
- Rapid weathering is driven by pyrite oxidation to sulfuric acid, followed by neutralization of the acid by primarily carbonate minerals
- The resulting weathering products lead to a globally distinct chemical signature for mining-impacted rivers and net efflux of rock CO₂

Supporting Information:

- Supporting Information S1

Correspondence to:

M. R. V. Ross,
matt.ross@colostate.edu

Citation:

Ross, M. R. V., Nippgen, F., Hassett, B. A., McGlynn, B. L., & Bernhardt, E. S. (2018). Pyrite oxidation drives exceptionally high weathering rates and geologic CO₂ release in mountaintop-mined landscapes. *Global Biogeochemical Cycles*, 32, 1182–1194. <https://doi.org/10.1029/2017GB005798>

Received 7 SEP 2017

Accepted 31 MAY 2018

Accepted article online 15 JUL 2018

Published online 15 AUG 2018

Pyrite Oxidation Drives Exceptionally High Weathering Rates and Geologic CO₂ Release in Mountaintop-Mined Landscapes

Matthew R. V. Ross¹ , Fabian Nippgen² , Brooke A. Hassett³, Brian L. McGlynn³ , and Emily S. Bernhardt¹ 

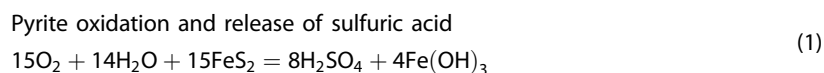
¹Department of Ecosystem Science and Sustainability, Colorado State University, Fort Collins, CO, USA, ²Department of Ecosystem Science and Management, University of Wyoming, Laramie, WY, USA, ³Division of Earth and Ocean Sciences, Nicholas School, Duke University, Durham, NC, USA

Abstract Weathering is the ultimate source of solutes for ecosystems, controls chemical denudation of landscapes, and drives the geologic carbon cycle. Mining and other land-moving operations enhance physical weathering by bringing large volumes of shattered bedrock to the surface. Yet, the relative influence of these activities on chemical weathering remains poorly constrained. Here we show that catchments impacted by mountaintop removal coal mining have among the highest rates of chemical weathering ever reported. Mined catchments deliver more than 7,600 kg·ha⁻¹·year⁻¹ of dissolved solids downstream. The chemical signatures of these exceptionally high weathering rates reflect the product of sulfuric acid weathering of carbonate-bearing rock, driven by the oxidation of pyritic materials. As this strong acid rapidly weathers surrounding carbonate materials, H⁺ ions are consumed and Ca²⁺, Mg²⁺, and HCO₃⁻ ions are exported to balance the elevated SO₄²⁻ exports, generating alkaline mine drainage. The sulfate exports from pyrite oxidation in mountaintop-mined catchments account for ~5–7% of global sulfate derived from pyrite, despite occupying less than 0.006% of total land area. Further, the suite of weathering reactions liberate 100–450 kg of rock-derived C·ha⁻¹·year⁻¹ as CO₂, with an additional 90–150 kg C·ha⁻¹·year⁻¹ of C released when HCO₃⁻ reaches the ocean. This rock C release contributes to the high carbon costs of coal combustion.

Plain Language Summary The reclaimed mountaintop removal coal mines of central Appalachia have exceptionally high weathering rates, with sulfuric acid weathering of carbonate rock releasing more than 4.5 million t of rock-derived solutes and at least 531,000 t of rock carbon as CO₂ each year.

1. Introduction

Chemical weathering of bedrock is typically dominated by carbonic acid weathering, which acts as a geologic sink of CO₂ (Dessert et al., 2003), ultimately regulating the carbon cycle over millennia (Maher & Chamberlain, 2014). However, when exposed to air or combusted, sulfur (S) compounds in coals and shales can be important sources of sulfuric acid (H₂SO₄, a strong weathering acid; Calmels et al., 2007; N. M. Johnson et al., 1972; Li et al., 2008; Raymond & Oh, 2009; Reynolds & Johnson, 1972; Torres et al., 2014; Xu & Liu, 2007). Substantial research documents that the CO₂ (Maher & Chamberlain, 2014) and SO₂ derived from coal combustion enhances regional and global weathering rates (N. M. Johnson et al., 1972; Lerman et al., 2007; Li et al., 2008; Xu & Liu, 2007), but little work has examined how weathering may be altered in the mines from which coal is extracted (though see Raymond & Oh, 2009). Mine operations expose large volumes of pyritic minerals (FeS₂-bearing rock) bringing these reduced materials into contact with air and water, generating sulfuric acid and oxidized iron (equation (1)).



Raymond and Oh (2009) estimated that escalation of this process by deep coal mining may account for 28–40% of modern global riverine S fluxes from pyrite oxidation.

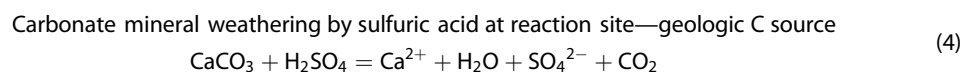
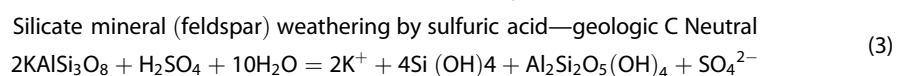
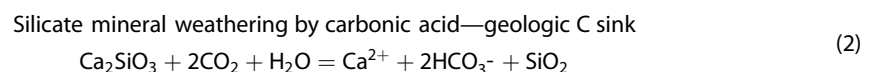
Before 1970, U.S. coal was primarily produced from underground mines (Lutz et al., 2013), which altered weathering patterns in mined areas by simply exposing FeS₂ to water and air (Raymond & Oh, 2009). Since 1970, coal production has been dominated by surface mining operations. In addition to exposing acid-generating FeS₂ to oxygen, surface mining also mechanically fragments large volumes of overlying

bedrock. Mountaintop removal coal mining with valley fills as practiced in Central Appalachia is a particularly extreme form of surface mining, excavating ridges as deep as 200 m and burying adjacent valleys and streams beneath many meters of highly heterogeneous fractured bedrock (Greer et al., 2017) and coal residues (Ross et al., 2016). These impacts are extensive (Drummond & Loveland, 2010; Townsend et al., 2009), covering more than 5,900 km² in central Appalachia (Pericak et al., 2018).

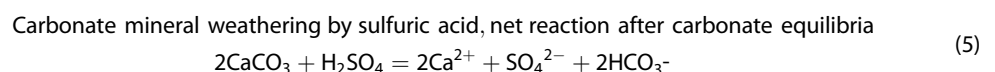
Postmining landscapes have lower slopes (Maxwell & Strager, 2013; Ross et al., 2016), increased water storage potential (Barbour et al., 2016; Ross et al., 2016; Wunsch et al., 1999), altered hydrologic flowpaths (Greer et al., 2017; Messinger & Paybins, 2003; Miller & Zégre, 2014; Nippgen et al., 2017; Zegre et al., 2014), and acid-generating pyrite in the particularly reactive form of small pyrite particles (Clark et al., 2018). Pyrite-bearing rocks are intentionally mixed with acid-neutralizing carbonate-bearing bedrock (Odenheimer et al., 2014) to prevent acid mine drainage. The physical fragmentation of bedrock alone likely leads to elevated weathering rates due to an increase in exposed surface area (equation (2)) as seen for rapidly weathering glacial till deposits (Calmels et al., 2007; Hilton et al., 2014; Lyons et al., 2005; Torres et al., 2017).

In mountaintop mining overburden deposits, a suite of chemical reactions generate alkaline mine drainage (Griffith et al., 2012; Lindberg et al., 2011). The production of alkaline mine drainage is initiated by FeS₂ dissolution and oxidation (equation (1)), generating sulfuric acid (Silverman & Ehrlich, 1964). This sulfuric acid can be neutralized through either silicate or carbonate weathering reactions (Clark et al., 2018). While the fill material across much of Central Appalachia is predominately silicate minerals (Clark et al., 2018), the alkaline mine drainage characteristic of coal mines in this region has been attributed to enhanced carbonate weathering of CaCO₃ and MgCO₃ (Banks et al., 1997; Daniels et al., 2016; Hawkins, 2004; Zhang et al., 1995). Together, these reactions liberate soluble ions previously held in bedrock (SO₄²⁻, Ca²⁺, Mg²⁺, HCO₃⁻, K⁺, Na⁺, and Cl⁻), which collectively increase both the pH and specific conductance of mine water effluent (Bernhardt et al., 2012; Griffith et al., 2012; Lindberg et al., 2011; Orndorff et al., 2015).

While both silicate and carbonate weathering reactions contribute to high solute concentrations of mining effluent, they have quite different implications for carbon cycling (equations (2)–(5) and Figure 1). In the absence of strong acids, weathering of silicates can be a substantial net carbon sink (equation (2)) over geologic timescales (Hamilton et al., 2007; Louvat & Allègre, 1997). In contrast, strong acid weathering of silicates is carbon neutral (equation (3)) and can liberate fossil carbon from carbonate rock weathering (equation (4)), with the CO₂ released from this reaction balanced by million-year timescales of sulfate reduction (Calmels et al., 2007; Li et al., 2008). The fate of this liberated C depends on solution pH, with CO₂ gas from equation (4) equilibrating with HCO₃⁻, a pH-dependent process (equations (4) and (5); Stumm & Morgan, 1996). In the heterogeneous reaction matrix of a valley fill (Greer et al., 2017), weathering reactions are occurring at the interface between pyrite, silicate, and carbonate minerals generating both acidic and basic conditions along the weathering fronts (Figure 1), with the aggregate result generating alkaline mine drainage (Lindberg et al., 2011). The following equations show carbonate weathering with calcium carbonate and silicate weathering with potassium feldspars, but replacing calcium with magnesium or potassium with sodium yields the same acid-neutralizing results.



Under alkaline conditions, much of this CO₂ is converted to HCO₃⁻ via carbonate equilibrium reactions (Stumm & Morgan, 1996), which yields the following net reaction (5):



Bicarbonate ions released by this weathering reaction (equation (5)) will be exported downstream with other weathering products but may also be evaded as CO₂ when waters become less alkaline downstream (Marcé

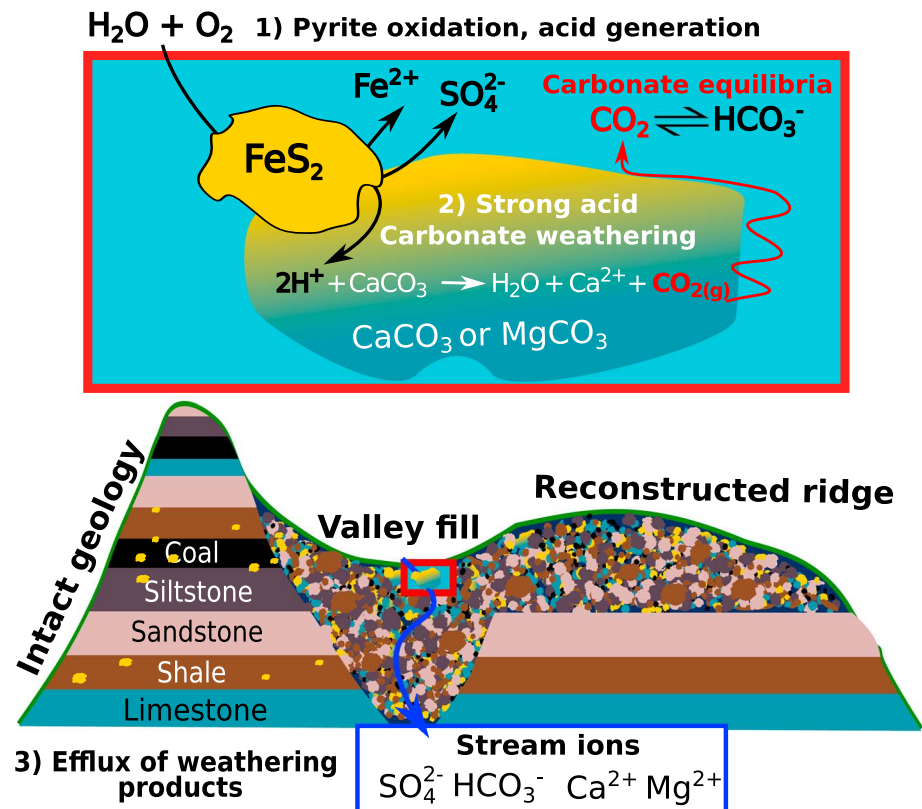
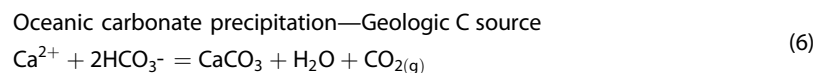


Figure 1. Conceptual diagram of valley fill structure and weathering reactions: Diagram shows the theoretical structure of a mountaintop-mined landscape and the chemical reactions that generate high concentrations of weathering products and high specific conductance in mined catchments. These reactions start with the oxidation and dissolution of pyrite particles (1) and the subsequent weathering of carbonate minerals by strong acid (2). Acidic conditions at the reaction site produce gaseous CO_2 , which evades into solution, producing bicarbonate (HCO_3^-). The net reaction produces a suite of weathering products, with the dominant ions being SO_4^{2-} , HCO_3^- , Ca^{2+} , and Mg^{2+} shown in (3). These weathering products are either generated and/or routed through valley fills, where they leave the system as dissolved ions in streams.

et al., 2015). Mining-derived HCO_3^- that enters the ocean can act as a CO_2 source over geologic timescales that occur over 10^6 years (Torres et al., 2014, 2017) via



Despite ample research on the high concentrations of rock-derived ions in streams draining mountaintop mines, there has been insufficient research on chemical weathering fluxes and almost no work looking at elevated pyrite oxidation and carbonate weathering effects on the geologic C cycle. Here we use a paired-catchment approach to estimate the impact of mountaintop mining on weathering rates and geologic C cycling.

2. Methods

2.1. Sites and Data Collection

This study was conducted in West Virginia's Mud River basin, where the Hobet surface mine is the primary form of landuse change with little history of deep mining (Messinger & Paybins, 2003) and only small amounts of low-density rural development (Figure 2, <https://mtm-weathering.web.duke.edu>). The Mud River basin covers three similar coal-bearing geologies: the Kanawha Formation, the Conemaugh Group, and the Allegheny formation. These formations are generally sequences of sandstone, siltstone, shale, limestone, and coal, with little or no marine sediments and primarily made up of carbonates and silicate minerals (Ehlke et al., 1982). Mixed hardwood forests dominate unmined portions of the landscape, while

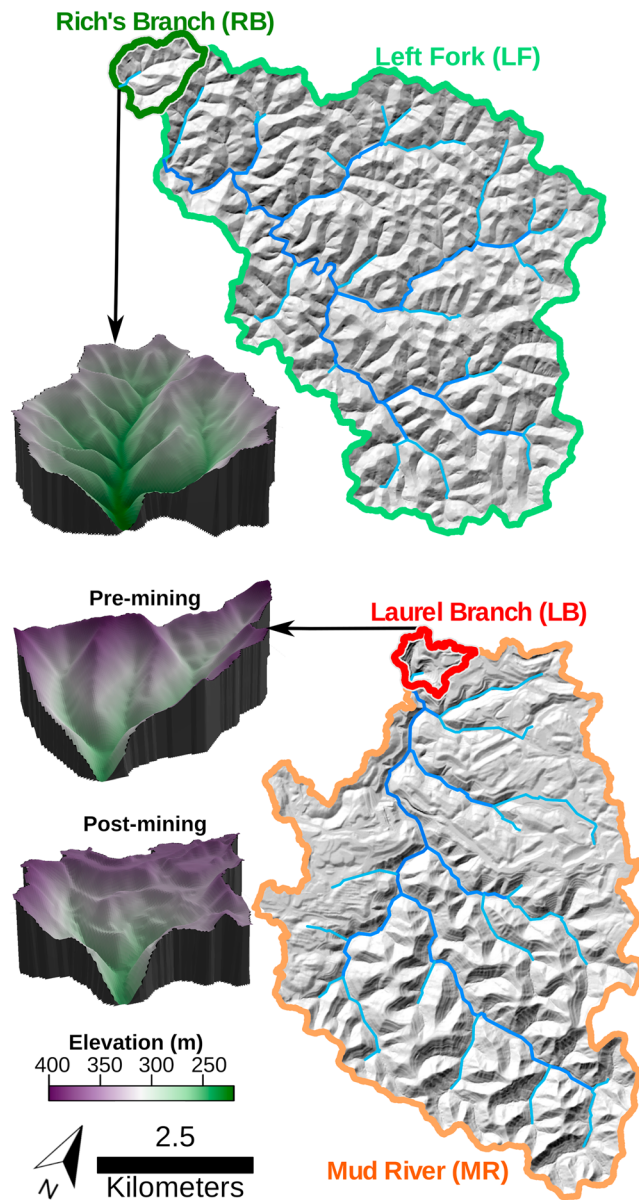


Figure 2. Study map: Hillshade maps of study sites. Reference catchments (RB and LF) are outlined in green, while red and orange highlight the mined catchments (LB and MR), and blue indicates stream lines. Sensors were placed at watershed outlets and samples taken at the same points. Insets show digital elevation model of first-order catchments with topographic changes shown at Laurel Branch (LB) with premining and postmining digital elevation models.

postmining landscapes are generally covered in grassland/shrublands with limited forest recovery (Zipper et al., 2011). Average annual rainfall is ~ 1100 mm distributed evenly throughout the year.

We monitored changes associated with mining at two different spatial scales (Figure 2). At the headwater scale, we compared the unmined Rich's Branch (RB, 118 ha, mean slope 19.5°) to the mined Laurel Branch (LB, 68 ha, mean slope 13.3°). Laurel Branch was 97 ha before mining activities deposited 10–14 million m^3 of spoil into the valley, shrinking the catchment area by 30% and lowering the mean slope by 7.5° from a premining 20.5° (Ross et al., 2016). At the fourth-order scale, we compared the reference site, Left Fork (LF, 3,463 ha, mean slope 17.5°), to the partially mined Mud River catchment (MR, 3,672 ha, mean slope 18.9°). Nearly half of MR (46%) has been heavily altered by mining with an estimated 162–185 million m^3 of spoil deposited into its headwater valleys, resulting in a decrease in mean slope of 3° and an increase of mean elevation by 2 m. These extensive topographic alterations are consistent with changes throughout the region (Ross et al., 2016). LB was mined from 2003 to 2010, and various parts of MR were mined from 1985 to 2015, with most mining operations in the two catchments completed by 2010.

We measured water level, conductivity (specific conductance in microsiemens per centimeter), and temperature at 10-min intervals from 1 October 2014 to 30 September 2015. Rating curves were developed for each stream to convert water level data to streamflow (see Nippen et al., 2017 for details). Specific conductance data at all sites had periods of drift due to either deposition of dissolved particulates onto the sensor electrodes or through partial sand burial. To correct for this sensor drift, we assumed linear drift from the previous download and corrected specific conductance to a handheld meter that was calibrated monthly.

We collected bulk surface water samples biweekly from each site along with pH measurements using a handheld probe. This regular sampling effort was supplemented with intensive storm sampling for six storms. All water samples were filtered through a $0.45\text{-}\mu\text{m}$ mixed-cellulose fiber filter and stored at 4°C prior to analysis. All samples were analyzed for SO_4^{2-} , Ca^{2+} , Mg^{2+} , K^+ , Na^+ , NO_3^- , and Cl^- using simultaneous anion and cation analysis on two Dionex ICS-2000 ion chromatographs with an AS-40 autosampler (Dionex, Sunnyvale, CA). Anions were analyzed on AS-18 guard and analytical columns. Minimum detection was 10 ppb for Cl^- and SO_4^{2-} and 3 ppb for NO_3^- . Cations were analyzed on CS-12A guard and analytical columns. Minimum detection was 0.3 ppm for Ca^{2+} , Mg^{2+} , and Na^+ and 30 ppb for K^+ . All samples with SO_4^{2-} concentrations greater than 200 ppm were diluted prior to analysis. Dissolved Si was determined by inductively coupled plasma-mass spectrometry for a subset of 50 samples collected from each site that were chosen to represent the full range of observed hydrologic conditions.

2.2. Data Analysis

Bicarbonate concentrations for each sample were calculated by charge equivalence, assuming that all unmet negative charge could be attributed to HCO_3^- , such that in equivalents per liter,

$$[\text{HCO}_3^-] = \Sigma\text{cations} - \Sigma\text{anions}$$

For this equation cations are Na^+ , K^+ , Mg^{2+} , and Ca^{2+} , and anions are SO_4^{2-} , Cl^- , and NO_3^- . We performed this calculation individually on every sample. Assuming all unmet charge is accounted for by HCO_3^- is a

pH-dependent assumption (Stumm & Morgan, 1996), but pH data from this study and more than 14 years of prior work in the study catchments suggests that pH in both reference and mined catchments is consistently between 6.8 and 8 (supporting information [SI] Figure S1), where unmet negative charge should be predominantly captured by HCO_3^- .

We used the ratio of sulfate to bicarbonate ions to infer dominant weathering sources. Carbonate weathering with full equilibration of CO_2 to HCO_3^- (equations (4) and (5)) should generate $\text{HCO}_3^-:\text{SO}_4^{2-}$ balanced at a 2:1 ratio. Solute yields well above this 2:1 ratio can only be achieved through carbonate weathering by carbonic acid, which sequesters CO_2 (equation (2)). In contrast, solute yields with a $\text{HCO}_3^-:\text{SO}_4^{2-}$ well below 2:1 are consistent with CO_2 production from strong acid weathering of carbonate rock (equation (4)). In the latter case, we can further assume that for each mole of excess SO_4^{2-} exported, 1 M of CO_2 must be produced (molar ratio of 1:1, equation (3)). We can then use this relationship to calculate rock weathering CO_2 efflux. This approach allows us to assess weathering reactions regardless of stream water pH, which integrates across the heterogeneous pH conditions found throughout the valley fill (see Figure 1). In addition to acid neutralization through carbonate weathering (equations (4) and (5)), silicate minerals can also neutralize sulfuric acid as in equation (3). As a result, we first account for Na^+ and K^+ with SO_4 at a 1:1 ratio before assessing the $\text{HCO}_3^-:\text{SO}_4^{2-}$ ratio.

We also used a second approach to estimate CO_2 sink strength from the relationships between major cations and HCO_3^- concentrations (equation (7), Hamilton et al., 2007).

$$[\text{CO}_2 \text{ sink strength}] \% = [\text{HCO}_3^- - 0.5(\text{Ca}^{2+} + \text{Mg}^{2+})] / [0.5(\text{Ca}^{2+} + \text{Mg}^{2+})]^* 100 \quad (7)$$

The dominant solutes in stream water are notably consistent over time and are strongly correlated with stream water specific conductance and discharge. Element concentration samples were taken every other week throughout the year with additional storm sampling. These data are well suited to a regression approach for estimating ion concentrations with sensor data, allowing predictions of ion concentrations at 10-min intervals. We tested multiple regression approaches between grab sample solute concentrations and in situ specific conductance and discharge. These approaches include modeling element concentration as a function of natural log of discharge, specific conductance, log discharge and specific conductance, and specific conductance and percent baseflow contribution (from Nippgen et al., 2017). Compared to simple flow-weighted mean estimates of element flux, the resulting concentration estimates provide higher temporal resolution data, more accurate estimates, and uncertainty bounds (Appling et al., 2015) on the flux of weathering products.

All analyses were completed using R statistical software, primarily the tidy data framework and associated packages (Wickham, 2011, 2014) in addition to the linear modeling built into R.

3. Results and Discussion

Stream water chemistry from unmined catchments indicates weathering of silicate and carbonate materials (Gaillardet et al., 1999), consistent with weathering of mixed sandstone and limestone bedrock (Gaillardet et al., 1999; Dessert et al., 2003; Xu & Liu, 2007; Figure 3b). The observed increases in Mg:Na and Ca:Na ratios in our mined catchments place the chemistry of receiving streams outside of the range of a global database of stream and river waters (Dessert et al., 2003; Gaillardet et al., 1999; Xu & Liu, 2007), indicating that mining is dramatically enhancing carbonate weathering, with higher amounts of Mg potentially released from chlorite weathering (Clark et al., 2018). Mining clearly elevates concentrations of carbonate weathering products (Ca^{2+} and Mg^{2+}), but direct measurements of silicate weathering rates show that mean Si concentration does not differ between mined and unmined sites (Figure 3c). However, elevated concentrations of Na^+ and K^+ in mined sites indicate an increase in K-feldspar and Na-feldspar silicate weathering, as suggested in previous work (Clark et al., 2018). The high concentrations of Na^+ and K^+ , but low Si concentrations suggest that while silicate minerals are being weathered, Si is remineralized before export in stream water. The highest mean concentrations of Si were observed in RB, the first-order reference catchment, where the Conemaugh Group, which is higher in sandstone, comprises more of the geology than all other sites. By promoting ideal conditions for strong acid weathering of carbonate rocks, mining shifts these catchments from silicate/carbonate weathering CO_2 sinks to strong acid carbonate weathering CO_2 sources (equation (7) and Figure 3d).

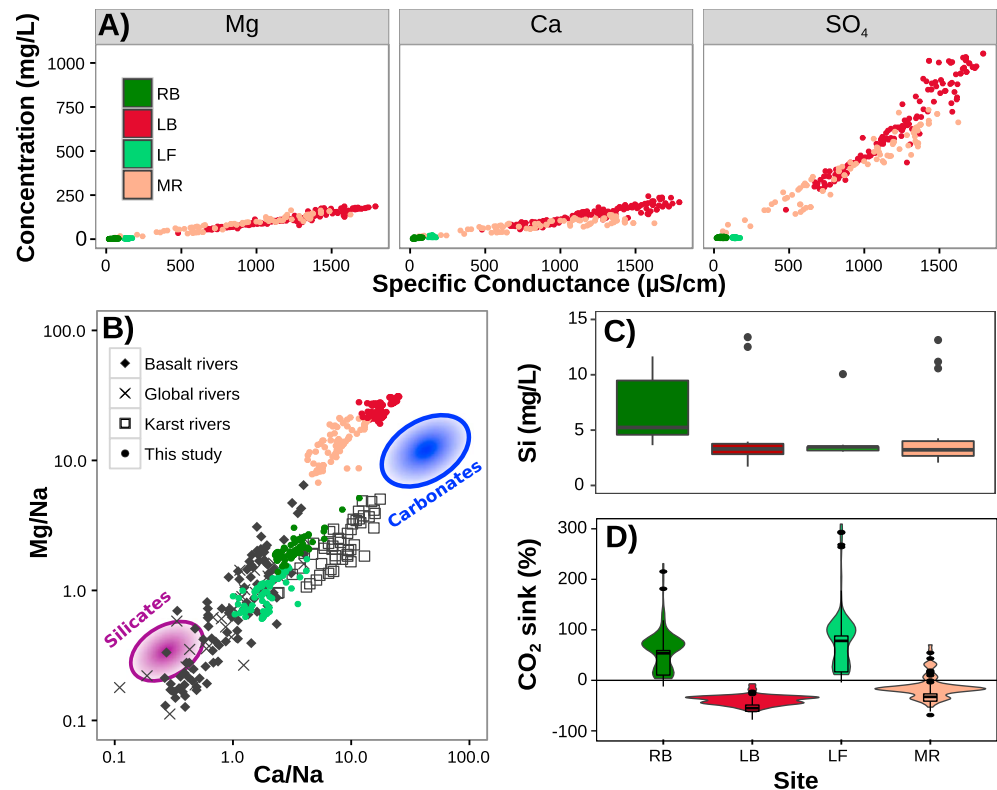


Figure 3. Specific conductance and ion correlations, weathering rates, and CO₂ sink strength: (a) correlation between specific conductance and individual ion concentrations at all sites from biweekly samples and three storms. These relationships, along with baseflow indices, were used to calculate daily flux estimates. (b) Na-normalized ratio of Ca and Mg from this study (plotted in circle colored points) and a synthesis of global stream water chemistry; crosses (x) denote global large rivers (Gaillardet et al., 1999), open squares denote karstic streams (Xu & Liu, 2007), and basalt streams are shown as closed diamonds (Dessert et al., 2003). The blue and purple circles indicate a range of ratios from pure carbonic acid weathering of carbonate and silicates, respectively (from Gaillardet et al., 1999). Note that the reference catchments have a mix of silicate and carbonate weathering signals, while the mined catchments clearly shift to being dominated by carbonate weathering ratios (high Mg and Ca). (c) Boxplot of dissolved Si concentrations from storm and baseflow samples at all sites, showing no statistical difference between mined and unmined Si concentration. (d) Violin plots with relative CO₂ sink strength as inferred from stream water chemistry (see text for details); negative values indicate that weathering was a source of CO₂ (equation (7)). RB = Rich's Branch; LB = Laurel Branch; LF = Left Fork; MR = Mud River.

There were strong positive correlations (SI Figure S2) between stream-specific conductance, natural log of discharge, percent baseflow contribution, and major ion concentration at all sites during both stormflow and baseflow (Ca²⁺, Mg²⁺, and SO₄²⁻; Figure 3a). To provide robust estimates of elemental flux, we compared four different types of linear models that predict element concentration based on sensor data measured at 10-min intervals. We used two methods to choose the best modeling approach. First, we built linear models using 70% of the data for each site, and, using the remaining 30% of data, we calculated the median absolute percent error by comparing observed element concentrations versus predicted. All models generally had errors <20%. The model where element concentration depends on specific conductance and percent baseflow had the lowest average error across all sites and elements (SI Figure S3, average error 14%). Secondly, we calculated the annualized flux of elements using the four different models by multiplying concentration by discharge and integrating over the study period. By comparing these models, we tested how sensitive the estimates of flux were depending on modeling approach. Our estimates of annual flux were robust across all four model formulations (Figure 4), with consistent estimates of flux across sites and elements. Using the lowest error model allowed us to use specific conductance and percent baseflow as a proxy for all individual ions at all sites ($R^2 > 0.65$, SI Table S1), effectively providing an estimate of ion concentrations at 10-min intervals for the entire water year (see SI Table S1 for R^2 and equations for all reported elemental concentrations). For presentation purposes, we took daily averages to display

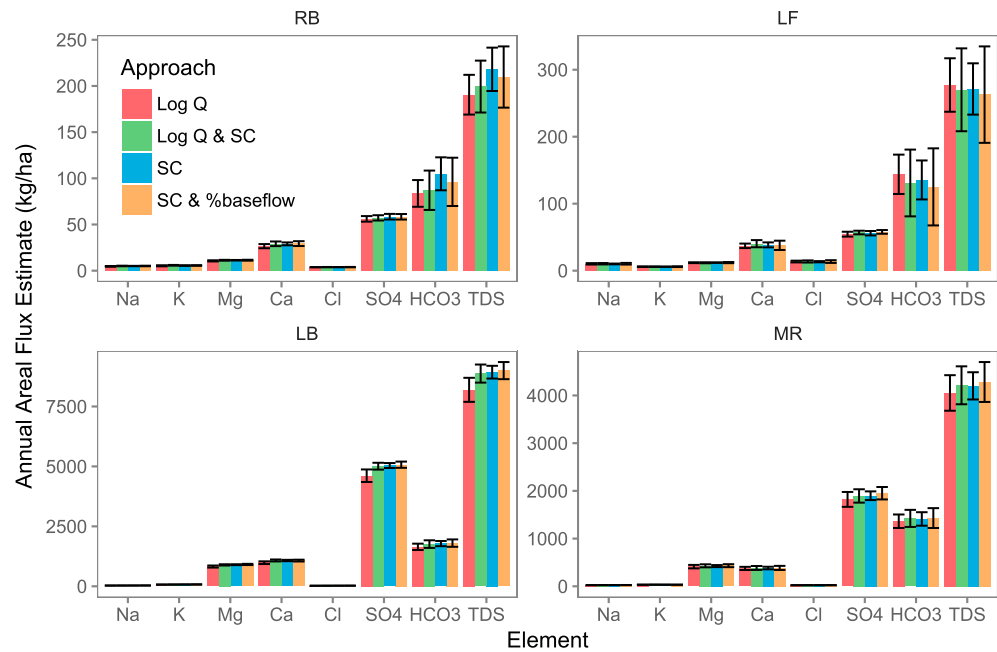


Figure 4. Annual flux of major weathering products using different modeling approaches: Bar plots show annualized element flux estimates in kilograms per hectare using four different modeling approaches: Log Q, Log Q & SC, SC, and SC & %baseflow, where Q is discharge in millimeters per hour and SC is specific conductance in microsiemens per centimeter. The 90% confidence interval estimates are shown as black lines with hashes at the end. Notice that the axis changes between each plot, and flux estimates are substantially similar regardless of modeling approach. The final modeling approach used in this study and for all subsequent figures was elements as a function of specific conductance (SC) and the percent baseflow (%baseflow) (Nippgen et al., 2017). RB = Rich’s Branch; LB = Laurel Branch; LF = Left Fork; MR = Mud River.

elemental flux data. With these estimates, we assumed that all unmet negative charge in modeled element concentration was met by HCO_3^- (SI Figure S4).

Across all sites NO_3^- was not predictable using the simple models of specific conductance and baseflow, likely because NO_3^- export is strongly influenced by biotic factors such as season and temperature, and therefore we excluded it from the annual analyses. For charge-balance purposes, NO_3^- made up less than 1% of total charge in all samples across all sites, so it has negligible impact on the calculations of HCO_3^- .

Similarly, previous work in the same study area has shown that dissolved organic carbon and metal concentrations make up less than 5% of the charge balance and likely have a small impact on the annualized HCO_3^- estimates (dissolved organic carbon ranged from 1.7 to 8.1 mg/L in Lindberg et al., 2011).

In the two unmined catchments, many elements (Ca^{2+} , Mg^{2+} , K^+ , and SO_4^{2-}) were exported at nearly the same area-adjusted rates. At the first-order reference, RB, total weathering products were exported at rates of $203 \pm 40 \text{ kg}\cdot\text{ha}^{-1}\cdot\text{year}^{-1}$, while the fourth-order reference, LF, exported solutes at rates of $247 \pm 71 \text{ kg}\cdot\text{ha}^{-1}\cdot\text{year}^{-1}$ (Table 1 and Figures 4 and 5, <https://mtm-weathering.web.duke.edu>). The similarity in areal export rates between the unmined headwater and fourth-order catchment suggests that natural weathering processes and routing of precipitation are similar between these unmined sites regardless of catchment size (Figure 5). The first order fully mined catchment, LB, exported 44 times more weathering solutes than its reference counterpart RB ($8,939 \pm 325 \text{ kg}\cdot\text{ha}^{-1}\cdot\text{year}^{-1}$). MR, the larger, mined catchment (46% mined), exported 15 times more solutes than its paired reference site LF ($3,703 \pm 442 \text{ kg}\cdot\text{ha}^{-1}\cdot\text{year}^{-1}$). If we assume that the 54% of MR that is unmined has weathering rates similar to the

Table 1
Annual Ion Flux Estimates Across Sites and the Ratio of Flux (Mined:Unmined)

Element	Site annual element flux (kg/ha)				First-order watershed ratio	Fourth-order watershed ratio
	LB	MR	RB	LF	Mined/unmined	Mined/unmined
Ca	1,095	365	30	36	36.5	10.1
Cl	27	22	4	14	6.8	1.6
HCO_3^*	1,602	919	90	111	17.8	8.3
K	82	32	6	6	13.7	5.3
Mg	929	431	11	12	84.5	35.9
Na	34	23	5	10	6.8	2.3
SO_4	5,170	1,911	57	58	90.7	32.9
TDS*	8,939	3,703	203	247	44	15

* HCO_3 flux estimates shown here is calculated where all unmet negative charge is assumed to be met by HCO_3 . LB = Laurel Branch; MR = Mud River; RB = Rich’s Branch; LF = Left Fork; TDS = total dissolved solids.

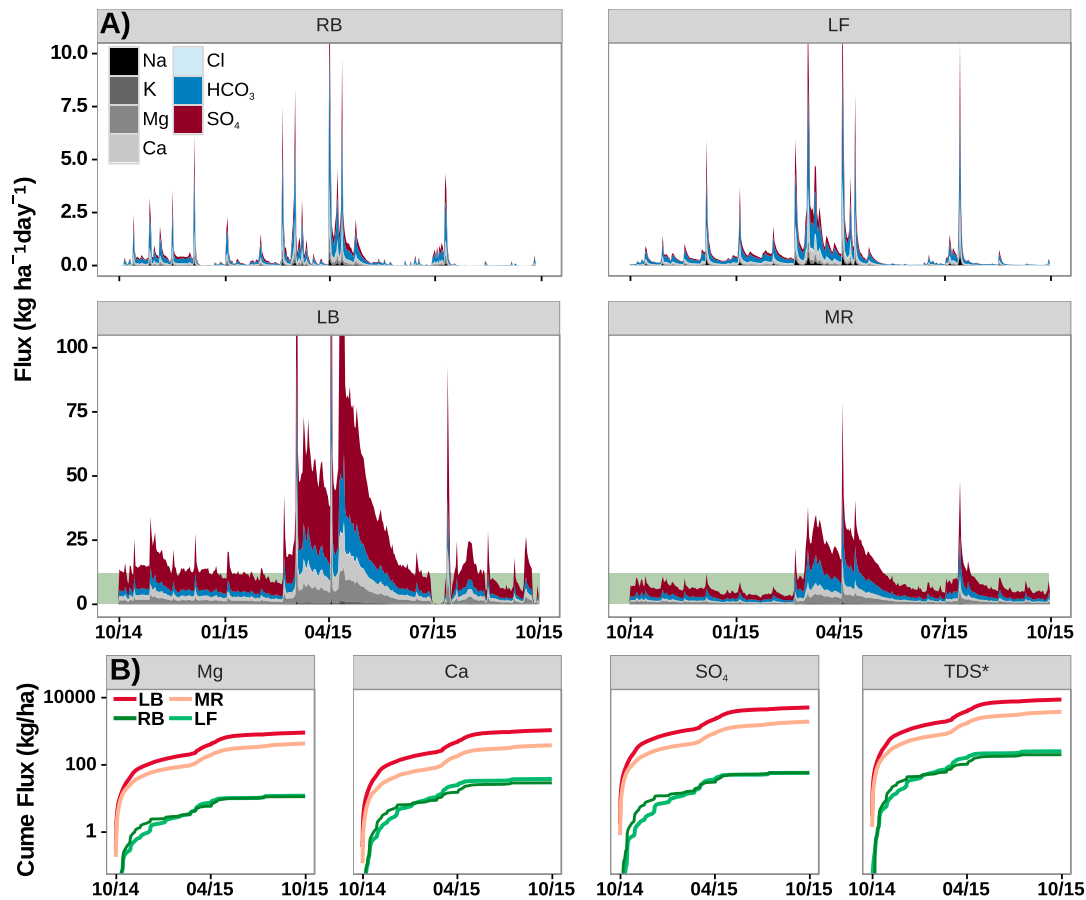


Figure 5. Daily flux of major weathering products: (a) modeled daily flux of major ions from the four study sites (see text for modeling details). Please note different y axes scaling between reference and mined sites. Green shading in LB and MR denotes the y axis scale of the reference sites. HCO_3^- was calculated by assuming charge balance. (b) Cumulative flux of major ions and TDS by site. Reference sites have nearly identical per-area flux, which obscures the LF line at times. RB = Rich's Branch; LB = Laurel Branch; LF = Left Fork; MR = Mud River; TDS = total dissolved solids.

reference catchments, we can then estimate that the mined portion of the catchment exported dissolved solutes at rates of $\sim 7,600 \pm 961 \text{ kg}\cdot\text{ha}^{-1}\cdot\text{year}^{-1}$. As such, the total weathering rates at the two mined sites were nearly equivalent, given measurement uncertainty. Such similar rates of solute export occur even though MR drains a series of mines that range in age from 5 to 30 years old, while LB drains a single mine that is ~ 5 years old, suggesting similar weathering processes regardless of mine age, which is consistent with prior findings (Ross et al., 2016).

These are extremely high chemical weathering rates. Only a single catchment, the Waiho catchment in New Zealand, exports dissolved solutes at a higher rate ($11,900 \text{ kg}\cdot\text{ha}^{-1}\cdot\text{year}^{-1}$, Lyons et al., 2005). The Waiho river drains a glacier and has much higher specific water yield, exporting 7–10 times more water per area than our sites. These mountaintop mining catchments are exporting twofold to eightfold more weathering solutes than the highly reactive, fresh bedrock, and high runoff islands of Iceland (Louvat et al., 2008), Réunion (Louvat & Allègre, 1997), and Papua New Guinea (Gaillardet et al., 1999), whose reported chemical weathering rates are among the highest in the world ($1,100\text{--}3,380 \text{ kg}\cdot\text{ha}^{-1}\cdot\text{year}^{-1}$).

High weathering rates have often been associated with C sequestration—indeed weathering reactions in these steep, geologically young islands act as important geologic C sinks through carbonic acid weathering of silicate and carbonate rock, sequestering as much as $25 \text{ g C}\cdot\text{m}^{-2}\cdot\text{year}^{-1}$ (Dessert et al., 2003). In contrast, the high weathering rates in mined catchments is driven by sulfuric acid weathering of carbonate rock leading to a loss of rock C as CO_2 . It may initially seem hard to reconcile this strong acid weathering source with the alkaline pH observed in receiving streams (pH $\sim 7.1\text{--}8.3$, SI Figure S1), yet the observed $\text{HCO}_3^-:\text{SO}_4^{2-}$ ratios can only be explained by strong acid weathering of carbonate rock (Figure 6). Sulfuric acid weathering of

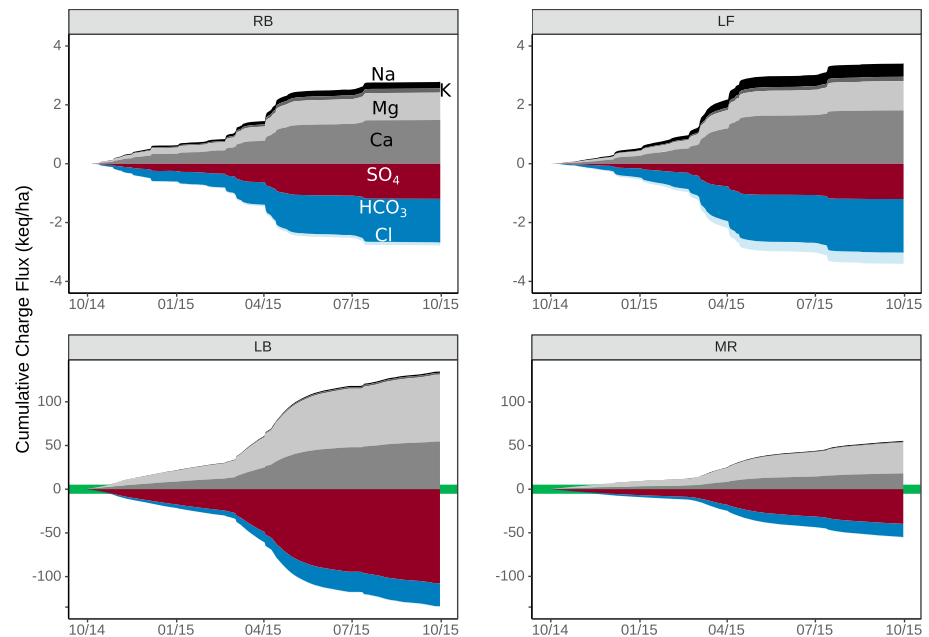


Figure 6. Cumulative charge flux: Shows cumulative ion flux (as kiloequivalents per hectare per year ($\text{keq}\cdot\text{ha}^{-1}\cdot\text{year}^{-1}$) for each site, with anions labeled in white (light blue = Cl) and cations labeled in black (dark gray = K). RB = Rich's Branch; LB = Laurel Branch; LF = Left Fork; MR = Mud River.

carbonates under alkaline conditions should produce a molar ratio of $\text{HCO}_3^-:\text{SO}_4^{2-}$ of 2:1; however, the ratio at the mined sites is 1:2, suggesting that there is far more SO_4^{2-} produced than can be accounted for by our estimates of HCO_3^- flux, even when accounting for neutralization of sulfuric acid through feldspar weathering (equations (3)–(5) and Figures 1 and 7). In contrast, the reference sites export HCO_3^- and SO_4^{2-} ions at a ratio closer to 2.7:1, suggesting that there is excess HCO_3^- produced by carbonic acid weathering, consistent with a weathering sink for CO_2 (equation (2) and Figure 7). When accounting for the potential for feldspar weathering to neutralize acidity from H_2SO_4 (equation (3)), we estimate that carbonic acid weathering in the unmined catchments sequesters $0.5\text{--}0.8\text{ g C}\cdot\text{m}^{-2}\cdot\text{year}^{-1}$ (Figure 7), while mined catchments are releasing rock C as CO_2 at rates of $10\text{--}45\text{ g}\cdot\text{m}^{-2}\cdot\text{year}^{-1}$. In the ocean, over a 10^6 -year timescale (Torres et al., 2014), bicarbonate released from sulfuric acid weathering in mined headwaters will reach the ocean and evade as CO_2 through equation (7), bringing the total C release rates up as high as $90\text{--}145\text{ g}\cdot\text{m}^{-2}\cdot\text{year}^{-1}$.

Previous estimates from the region suggest that mountaintop-mined coal produces 0.83 Mg C for every square meter of mined land (Lutz et al., 2013). It would take more than 5,000 years for the acid weathering C release to match the C released directly from coal combustion. However, fossil C release from weathering in mined catchments could offset 20–90% of annual net ecosystem C uptake by vegetation on mined lands (estimated at $167\text{--}389\text{ g C}\cdot\text{m}^{-2}\cdot\text{year}^{-1}$, Lutz et al., 2013). Since the release of weathering derived solutes persists for decades after mining ceases (Ross et al., 2016), oxidation of ancient rock-organic C bound up in coal residues and shales could dramatically increase our estimates of fossil C release from these mines (Hilton et al., 2014), especially when considering elevated oxidation of lithosphere C in rapidly weathering catchments (Hemingway et al., 2018). These additional carbon release pathways add substantially to previous estimates of the full carbon costs of coal (Campbell & Fox, 2010).

The high weathering rates and CO_2 efflux observed from mined catchments likely alters the physical structure of valley fills. For example, at LB, the loss of more than 700 t of material per year through downstream export of weathering products should create void spaces of $225\text{--}350\text{ m}^3$ annually, assuming that spoil material bulk density ranges from $2\text{ to }3\text{ g}/\text{cm}^3$ (Wunsch et al., 1999). If this void generation rate were applied evenly over the entire LB catchment, it would represent a chemical denudation rate of at least $330\text{ mm}/\text{kyr}$, a rate 55 times faster than the background estimates of chemical and physical denudation rates for Beryllium-10 derived rates in Appalachian mountains of $6 \pm 3\text{ mm}/\text{kyr}$ (Hancock & Kirwan, 2007).

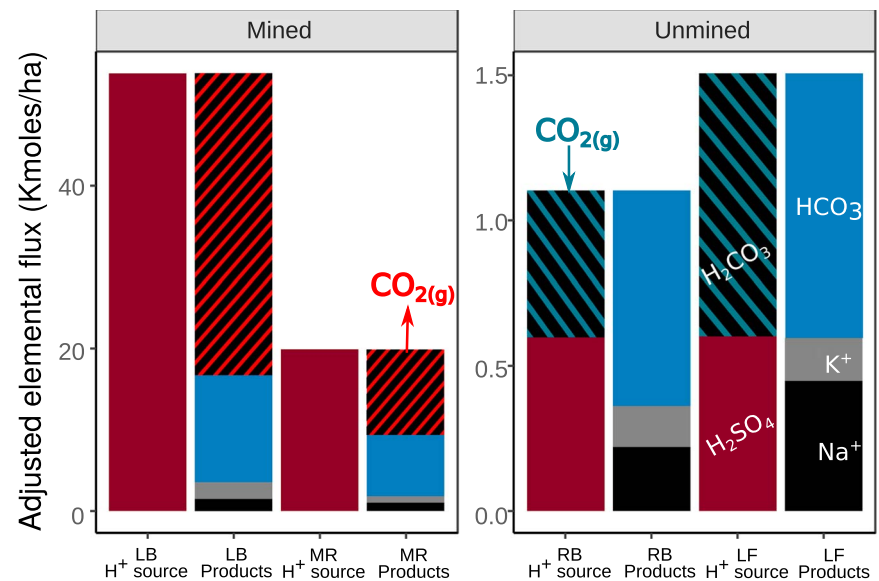


Figure 7. The amount of CO₂ evaded or sequestered from chemical weathering depends on weathering reactions as shown in equations (2)–(5). Sulfuric acid weathering of carbonates and silicates can be neutralized by equations (3)–(5), and by accounting for the net efflux of these weathering products (SO₄²⁻, HCO₃⁻, Na⁺, and K⁺) we can estimate the carbon consequences of weathering after adjusting for their molar ratios in equations (3)–(5). This graph shows that in mined catchments there is excess sulfate—from sulfuric acid, H₂SO₄, solid red bar—when compared to its balanced weathering products; we assume that all of this excess sulfate is balanced by CO₂ efflux to the atmosphere (black and red striped bars). The opposite is true in the unmined catchments, where there is not enough sulfate (expressed as H₂SO₄ in the plot) to explain the total weathering products. As a result, in the unmined catchments we assume the opposite is true: Additional weathering products are generated by silicate weathering with H₂CO₃ and CO₂ as the ultimate H⁺ source, making unmined catchments a net CO₂ sink. RB = Rich’s Branch; LB = Laurel Branch; LF = Left Fork; MR = Mud River.

By our estimate, at least 760 t of dissolved solids and ~90–145 t of geologic C are being released from each square kilometer of mines in the Mud River catchment per year. The solute concentrations and their ratios reported here are similar to other studies from the region (Griffith et al., 2012; Lindberg et al., 2011). Our rate estimates were also consistent between the small recently mined catchment and the larger catchment that includes areas mined progressively over the last four decades. These consistencies support scaling the results of the current study to the entire Central Appalachian coal-mining region. If we apply our measured weathering rates to the entire 5,900 km² of active, abandoned, and reclaimed mines (Pericak et al., 2018), we estimate that strong acid weathering of mine spoil could export more than 4.5 million tons of dissolved ions to regional rivers and release 531,000–855,000 t of geologic C as CO₂ annually.

Our regional estimates of chemical weathering rates and carbon release are conservative both regionally and globally. Pyrite and carbonate content—the chemical engines driving elevated weathering—is relatively low in this region with pyrite concentrations often not detectable in rock core samples (<1% of rock; Clark et al., 2018), and the county with our study sites has low carbonate concentrations compared to the other parts of Central Appalachia where it ranges from 1% to 13% (Clark et al., 2018). Furthermore, total sulfur content in the coal, another proxy for acid-weathering potential (Skousen et al., 2002), is on the low end (~1%) of the USA (0.5–5%, Casagrande, 1987) and global range (1–10%, Chou, 1997). These lower-end pyrite and carbonate concentrations still translate to very high weathering rates in our study system, but work in other parts of Appalachia have reported specific conductance values 2–10 times higher than reported here, suggesting much higher weathering rates are probable in the region (B. R. Johnson et al., 2010).

This regional impact has global consequences for the cycling of sulfur. While mountaintop mining operations in Central Appalachia cover less than 0.006% of the land area of Earth, they contribute a globally significant amount of sulfate to surface water through pyrite oxidation. Previous work estimates global, pyrite-derived sulfate weathering rates at 4.5–6.2 * 10¹³ g/year (Berner & Berner, 1996; Francois & Walker, 1992). Scaled to the 5,900 km² of mountaintop mined land in central Appalachia, we estimate that mine lands export 3.24 * 10¹² g/year of pyrite derived sulfate, accounting for 5–7% of the current global budget. Estimates of

worldwide pyrite oxidation rates are likely significant underestimates given more recent work showing similarly high pyrite oxidation rates in glaciated landscapes (Calmels et al., 2007; Torres et al., 2017), heavy rainfall catchments (Das et al., 2012), and deep mines (Raymond & Oh, 2009). Even if the global estimate increases substantially, the rates of pyrite oxidized sulfate production from mined Appalachian catchments will still be significant and highly disproportionate to their area. Lastly, increases in pyrite-driven weathering and the subsequent increase in bicarbonate flux will likely impact regional HCO_3^- flux and alkalization of rivers (Raymond & Hamilton, 2018).

More than 40% of the 5.6 billion tons of coal mined globally (Reichl et al., 2016) is derived from surface mining techniques (World Coal Institute, 2005). These coal mining activities will result in the liberation and oxidation of pyrite minerals, enhanced potential for strong acid weathering, the production of dissolved salts, and the release of geologically bound C. Unlocking geologically sequestered pyrite has important implications for global biogeochemical cycles of S, C, Ca, and Mg, whether it is the result of glaciers (Torres et al., 2017) or coal mines.

Acknowledgments

This research was funded by a National Science Foundation EAR Hydrologic Sciences grant 1417405 to B. L. McGlynn and E. S. Bernhardt and an NSF Graduate Research Fellowship to M. Ross. The staff of WV DNR District 5 Upper Mud River provided logistical support with special thanks to Nick Huffman. We would like to thank Anita and Stanley Miller for access to their property and field assistance and thank Brian Lutz for a thoughtful and helpful initial review of this manuscript. Steve Hamilton was vital to developing the ideas in this manuscript. Data, coarsened to daily means, for this paper can be found at the public GitHub repository for the interactive web application visualizing all data found in this manuscript. The address for the web application is <http://mtm-weathering.web.duke.edu/>, and the GitHub repository location is <https://github.com/matthewross07/MTM.Weathering>.

References

- Appling, A. P., Leon, M. P., & McDowell, W. H. (2015). Reducing bias and quantifying uncertainty in watershed flux estimates: The R package loadflex. *Ecosphere*, 6(12), 1–25. <https://doi.org/10.1890/ES14-00517.1.sm>
- Banks, D., Younger, P. L., Arnesen, R. T., Iversen, E. R., & Banks, S. B. (1997). Mine-water chemistry: The good, the bad and the ugly. *Environmental Geology*, 32(3), 157–174. <https://doi.org/10.1007/s002540050204>
- Barbour, S. L., Hendry, M. J., & Carey, S. K. (2016). High-resolution profiling of the stable isotopes of water in unsaturated coal waste rock. *Journal of Hydrology*, 534, 616–629. <https://doi.org/10.1016/j.jhydrol.2016.01.053>
- Berner, E., & Berner, R. (1996). *Global environment. Water, air, and geochemical cycles*. Englewood Cliffs, NJ: Prentice Hall.
- Bernhardt, E. S., Lutz, B. D., King, R. S., Fay, J. P., Carter, C. E., Helton, A. M., et al. (2012). How many mountains can we mine? Assessing the regional degradation of Central Appalachian rivers by surface coal mining. *Environmental Science & Technology*, 46(15), 8115–8122. <https://doi.org/10.1021/es301144q>
- Calmels, D., Gaillardet, J., Brenot, A., & France-Lanord, C. (2007). Sustained sulfide oxidation by physical erosion processes in the Mackenzie River basin: Climatic perspectives. *Geology*, 35(11), 1003–1006. <https://doi.org/10.1130/G24132A.1>
- Campbell, J. E., & Fox, J. F. (2010). Terrestrial carbon disturbance from mountaintop mining increases lifecycle emissions for clean coal. *Environmental Science & Technology*, 44(6), 2144–2149.
- Casagrande, D. J. (1987). Sulphur in peat and coal. *Geological Society, London, Special Publications*, 32(1), 87–105. <https://doi.org/10.1144/GSL.SP.1987.032.01.07>
- Chou, L. (1997). Geological factors affecting the abundance, distribution and speciation of sulphur in coals. In Q. Yang (Ed.), *Geology of Fossil Fuels – Coal, Proceedings of the 30th International Geological Congress* (Vol. 18, pt. B, pp. 47–57). VSP, Utrecht, Netherlands.
- Clark, E. V., Daniels, W. L., Zipper, C. E., & Eriksson, K. (2018). Mineralogical influences on water quality from weathering of surface coal mine spoils. *Applied Geochemistry*, 91(January), 97–106. <https://doi.org/10.1016/j.apgeochem.2018.02.001>
- Daniels, W. L., Zipper, C. E., Orndorff, Z. W., Skousen, J., Barton, C. D., McDonald, L. M., & Beck, M. A. (2016). Predicting total dissolved solids release from Central Appalachian coal mine spoils. *Environmental Pollution*, 216, 371–379. <https://doi.org/10.1016/j.envpol.2016.05.044>
- Das, A., Chung, C. H., & You, C. F. (2012). Disproportionately high rates of sulfide oxidation from mountainous river basins of Taiwan orogeny: Sulfur isotope evidence. *Geophysical Research Letters*, 39, L12404. <https://doi.org/10.1029/2012GL051549>
- Dessert, C., Dupré, B., Gaillardet, J., François, L. M., Allègre, C. J., Francois, L. M., & Allègre, C. J. (2003). Basalt weathering laws and the impact of basalt weathering on the global carbon cycle. *Chemical Geology*, 202(3–4), 257–273. <https://doi.org/10.1016/j.chemgeo.2002.10.001>
- Drummond, M. A., & Loveland, T. R. (2010). Land-use pressure and a transition to forest-cover loss in the eastern United States. *Bioscience*, 60(4), 286–298. <https://doi.org/10.1525/bio.2010.60.4.7>
- Ehlike, T. A., Runner, G. S., & Downs, S. C. (1982). Hydrology of Area 9, Eastern Coal Province, West Virginia. Water-resources investigations (USA).
- Francois, L. M., & Walker, J. C. G. (1992). Modelling the Phanerozoic carbon cycle and climate: Constraints from the $^{87}\text{Sr}/^{86}\text{Sr}$ isotopic ratio of seawater. *American Journal of Science*, 292(2), 81–135. <https://doi.org/10.2475/ajs.292.2.81>
- Gaillardet, J., Dupré, B., Louvat, P., & Allègre, C. J. (1999). Global silicate weathering and CO_2 consumption rates deduced from the chemistry of large rivers. *Chemical Geology*, 159(1–4), 3–30. [https://doi.org/10.1016/S0009-2541\(99\)00031-5](https://doi.org/10.1016/S0009-2541(99)00031-5)
- Greer, B. M., Burbey, T. J., Zipper, C. E., & Hester, E. T. (2017). Electrical resistivity imaging of hydrologic flow through surface coal mine valley fills with comparison to other landforms. *Hydrological Processes*, 31(12), 2244–2260. <https://doi.org/10.1002/hyp.11180>
- Griffith, M. B., Norton, S. B., Alexander, L. C., Pollard, A. I., & LeDuc, S. D. (2012). The effects of mountaintop mines and valley fills on the physicochemical quality of stream ecosystems in the Central Appalachians: A review. *The Science of the Total Environment*, 417–418, 1–12. <https://doi.org/10.1016/j.scitotenv.2011.12.042>
- Hamilton, S. K., Kurzman, A. L., Arango, C., Jin, L., & Robertson, G. P. (2007). Evidence for carbon sequestration by agricultural liming. *Global Biogeochemical Cycles*, 21, GB2021. <https://doi.org/10.1029/2006GB002738>
- Hancock, G., & Kirwan, M. (2007). Summit erosion rates deduced from ^{10}Be : Implications for relief production in the Central Appalachians. *Geology*, 35(1), 89. <https://doi.org/10.1130/G23147A.1>
- Hawkins, J. W. (2004). Predictability of surface mine spoil hydrologic properties in the Appalachian Plateau. *Ground Water*, 42(1), 119–125. <https://doi.org/10.1111/j.1745-6584.2004.tb02457.x>
- Hemingway, J. D., Hilton, R. G., Hovius, N., Eglinton, T. I., Haghpor, N., Wacker, L., et al. (2018). Microbial oxidation of lithospheric organic carbon in rapidly eroding tropical mountain soils. *Science*, 360(6385), 209–212. <https://doi.org/10.1126/science.aao6463>
- Hilton, R. G., Gaillardet, J., Calmels, D., & Birck, J. L. (2014). Geological respiration of a mountain belt revealed by the trace element rhenium. *Earth and Planetary Science Letters*, 403, 27–36. <https://doi.org/10.1016/j.epsl.2014.06.021>
- Johnson, B. R., Haas, A., & Fritz, K. M. (2010). Use of spatially explicit physicochemical data to measure downstream impacts of headwater stream disturbance. *Water Resources Research*, 46, W09526. <https://doi.org/10.1029/2009WR008417>

- Johnson, N. M., Reynolds, R. C., & Likens, G. E. (1972). Atmospheric sulfur: Its effect on the chemical weathering of New England. *Science*, 177(4048), 514–516. <https://doi.org/10.1126/science.177.4048.514>
- Lerman, A., Wu, L., & Mackenzie, F. T. (2007). CO₂ and H₂SO₄ consumption in weathering and material transport to the ocean, and their role in the global carbon balance. *Marine Chemistry*, 106(1–2 SPEC. ISS), 326–350. <https://doi.org/10.1016/j.marchem.2006.04.004>
- Li, S., Calmels, D., Han, G., Gaillardet, J., & Liu, C. (2008). Sulfuric acid as an agent of carbonate weathering constrained by $\delta^{13}\text{C}$ DIC: Examples from southwest China. *Earth and Planetary Science Letters*, 270, 189–199. <https://doi.org/10.1016/j.epsl.2008.02.039>
- Lindberg, T. T., Bernhardt, E. S., Bier, R., Helton, A. M., Merola, R. B., Vengosh, A., & Di Giulio, R. T. (2011). Cumulative impacts of mountaintop mining on an Appalachian watershed. *Proceedings of the National Academy of Sciences of the United States of America*, 108(52), 20,929–20,934. <https://doi.org/10.1073/pnas.1112381108>
- Louvat, P., & Allègre, C. J. (1997). Present denudation rates on the island of Réunion determined by river geochemistry: Basalt weathering and mass budget between chemical and mechanical erosions. *Geochimica et Cosmochimica Acta*, 61(17), 3645–3669. [https://doi.org/10.1016/S0016-7037\(97\)00180-4](https://doi.org/10.1016/S0016-7037(97)00180-4)
- Louvat, P., Gislason, S. R., & Allègre, C. J. (2008). Chemical and mechanical erosion rates in Iceland as deduced from river dissolved and solid material. *American Journal of Science*, 308(5), 679–726. <https://doi.org/10.2475/05.2008.02>
- Lutz, B. D., Bernhardt, E. S., & Schlesinger, W. H. (2013). The environmental price tag on a ton of mountaintop removal coal. *PLoS One*, 8(9), e73203. <https://doi.org/10.1371/journal.pone.0073203>
- Lyons, W. B., Carey, A. E., Hicks, D. M., & Nezat, C. A. (2005). Chemical weathering in high-sediment-yielding watersheds, New Zealand. *Journal of Geophysical Research*, 110, F01008. <https://doi.org/10.1029/2003JF000088>
- Maher, K., & Chamberlain, C. P. (2014). Hydrologic regulation of chemical weathering and the geologic carbon cycle. *Science*, 343(6178), 1502–1504. <https://doi.org/10.1126/science.1250770>
- Marcé, R., Obrador, B., Morgui, J., Riera, J. L., López, P., & Armengol, J. (2015). Carbonate weathering as a driver of CO₂ supersaturation in lakes. *Nature Geoscience*, 8(2), 107–111. <https://doi.org/10.1038/NGE02341>
- Maxwell, A. E., & Strager, M. P. (2013). Assessing landform alterations induced by mountaintop mining. *Natural Science*, 05(02), 229–237. <https://doi.org/10.4236/ns.2013.52A034>
- Messinger, T., & Paybins, K. S. (2003). Relations between precipitation and daily and monthly mean flows in gaged, unmined, and valley-filled watersheds, Ballard Fork, West Virginia, 1999–2001. Charleston, WV.
- Miller, A., & Zégre, N. (2014). Mountaintop removal mining and catchment hydrology. *Water*, 6(3), 472–499. <https://doi.org/10.3390/w6030472>
- Nippgen, F., Ross, M. R. V., Bernhardt, E. S., & Mcglynn, B. L. (2017). Creating a more perennial problem? Mountaintop removal coal mining enhances and sustains saline base flows of Appalachian watersheds. *Environmental Science & Technology*, 51(15), 8324–8334. <https://doi.org/10.1021/acs.est.7b02288>
- Odenheimer, J., Skousen, J., McDonald, L. M., Vesper, D. J., Mannix, M., & Daniels, W. L. (2014). Predicting release of total dissolved solids from overburden material using acid-base accounting parameters. *Geochemistry: Exploration, Environment, Analysis*, 15(2-3), 131–137. <https://doi.org/10.1144/geochem2014-276>
- Orndorff, Z. W., Daniels, W. L., Zipper, C. E., Eick, M., & Beck, M. (2015). A column evaluation of Appalachian coal mine spoils' temporal leaching behavior. *Environmental Pollution*, 204, 39–47. <https://doi.org/10.1016/j.envpol.2015.03.049>
- Pericak, A. A., Thomas, C. J., Kroodsma, D. A., Wasson, M. F., Ross, M. R. V., Clinton, N. E., et al. (2018). Mapping the yearly extent of surface coal mining in Central Appalachia using Landsat and Google Earth Engine. *PLoS One*, 13(7), 1–15. <https://doi.org/10.1371/journal.pone.0197758>
- Raymond, P. A., & Hamilton, S. K. (2018). Anthropogenic influences on riverine fluxes of dissolved inorganic carbon to the oceans. *Limnology and Oceanography Letters*, 3(3), 143–155. <https://doi.org/10.1002/lo.120069>
- Raymond, P. A., & Oh, N.-H. (2009). Long term changes of chemical weathering products in rivers heavily impacted from acid mine drainage: Insights on the impact of coal mining on regional and global carbon and sulfur budgets. *Earth and Planetary Science Letters*, 284(1–2), 50–56. <https://doi.org/10.1016/j.epsl.2009.04.006>
- Reichl, C., Schatz, M., & Zsak, G. (2016). World mining data 2016, 31, 1–255. Retrieved from <https://www.en.bmwfw.gv.at/Energy/Documents/WMD2016.pdf>
- Reynolds, R. C., & Johnson, N. M. (1972). Chemical weathering in the temperate glacial environment of the northern Cascade Mountains. *Geochimica et Cosmochimica Acta*, 36(5), 537–554. [https://doi.org/10.1016/0016-7037\(72\)90074-9](https://doi.org/10.1016/0016-7037(72)90074-9)
- Ross, M. R. V., McGlynn, B. L., & Bernhardt, E. S. (2016). Deep impact: Effects of mountaintop mining on surface topography, bedrock structure, and downstream waters. *Environmental Science & Technology*, 50(4), 2064–2074. <https://doi.org/10.1021/acs.est.5b04532>
- Silverman, M. P., & Ehrlich, H. L. (1964). Microbial formation and degradation of minerals. *Advances in Applied Microbiology*, 6. [https://doi.org/10.1016/S0065-2164\(08\)70626-9](https://doi.org/10.1016/S0065-2164(08)70626-9)
- Skousen, J., Simmons, J., McDonald, L. M., & Ziemkiewicz, P. (2002). Acid-base accounting to predict post-mining drainage quality on surface mines. *Journal of Environmental Quality*, 31(6), 2034–2044. Retrieved from <http://www.ncbi.nlm.nih.gov/pubmed/12469854>
- Stumm, W., & Morgan, J. J. (1996). Aquatic chemistry: Chemical equilibria and rates in natural waters. *Environmental Science and Technology*, 60(24), 5158–5159. [https://doi.org/10.1016/S0016-7037\(97\)81133-7](https://doi.org/10.1016/S0016-7037(97)81133-7)
- Torres, M. A., Moosdorf, N., Hartmann, J., Adkins, J. F., & West, A. J. (2017). Glacial weathering, sulfide oxidation, and global carbon cycle feedbacks. *Proceedings of the National Academy of Sciences of the United States of America*, 114(33), 8716–8721. <https://doi.org/10.1073/pnas.1702953114>
- Torres, M. A., West, A. J., & Li, G. (2014). Sulphide oxidation and carbonate dissolution as a source of CO₂ over geological timescales. *Nature*, 507(7492), 346–349. <https://doi.org/10.1038/nature13030>
- Townsend, P. A., Helmers, D. P., Kingdon, C. C., McNeil, B. E., de Beurs, K. M., & Eshleman, K. N. (2009). Changes in the extent of surface mining and reclamation in the Central Appalachians detected using a 1976–2006 Landsat time series. *Remote Sensing of Environment*, 113(1), 62–72. <https://doi.org/10.1016/j.rse.2008.08.012>
- Wickham, H. (2011). ggplot2. *Wiley Interdisciplinary Reviews: Computational Statistics*, 3(2), 180–185. <https://doi.org/10.1002/wics.147/full>
- Wickham, H. (2014). Tidy Data. *Journal of Statistical Software*, 59(10), 1–23. <https://doi.org/10.18637/jss.v059.i10>
- World Coal Institute (2005). The coal resource: A comprehensive overview of coal.
- Wunsch, D. R., Dinger, J. S., & Graham, C. D. R. (1999). Predicting ground-water movement in large mine spoil areas in the Appalachian Plateau. *International Journal of Coal Geology*, 41(1–2), 73–106. [https://doi.org/10.1016/S0166-5162\(99\)00012-9](https://doi.org/10.1016/S0166-5162(99)00012-9)
- Xu, Z., & Liu, C. (2007). Chemical weathering in the upper reaches of Xijiang River draining the Yunnan-Guizhou plateau. *Southwest China*, 239(1–2), 83–95. <https://doi.org/10.1016/j.chemgeo.2006.12.008>

- Zegre, N. P., Miller, A. J., Maxwell, A., & Lamont, S. J. (2014). Multiscale analysis of hydrology in a mountaintop mine-impacted watershed. *JAWRA Journal of the American Water Resources Association*, 50(5), 1257–1272. <https://doi.org/10.1111/jawr.12184>
- Zhang, Y. L., Evangelou, V. P., & Zhang, Y. L. (1995). A review: Pyrite oxidation mechanisms and acid mine drainage prevention. *Critical Reviews in Environmental Science and Technology*, 25(2), 141–199. <https://doi.org/10.1080/10643389509388477>
- Zipper, C. E., Burger, J. A., Skousen, J. G., Angel, P. N., Barton, C. D., Davis, V., & Franklin, J. A. (2011). Restoring forests and associated ecosystem services on Appalachian coal surface mines. *Environmental Management*, 47(5), 751–765. <https://doi.org/10.1007/s00267-011-9670-z>